This is to certify that the
thesis entitled

PRESSURE CORRECTION FOR INTERMEDIATE-PRESSURE STEAM TURBINE EFFICIENCY

presented by

DeVon A. Washington

has been accepted towards fulfillment
of the requirements for the

M.S. degree in Mechanical Engineering

Major Professor's Signature

11/30/04

Date

DATE DUE	DATE DUE	DATE DUE

PRESSURE CORRECTION FOR INTERMEDIATE-PRESSURE STEAM TURBINE EFFICIENCY

By

DeVon A. Washington

A THESIS

Submitted to
Michigan State University
In partial fulfillment of the requirements
for the degree of

MASTER OF SCIENCE

Department of Mechanical Engineering

2004

ABSTRACT

PRESSURE CORRECTION FOR INTERMEDIATE-PRESSURE STEAM TURBINE EFFICIENCY

By

DeVon A. Washington

For the power generation industry equipment performance is a major concern. The information obtained is not only used to ascertain the current condition of any particular piece of equipment, it is also used to forecast equipment maintenance and reliability. The accuracy of this information is vital. Small fluctuations in turbine efficiency can have considerable financial implications over the lifespan of the turbine; therefore, accurately monitoring efficiency is financially prudent.

Consumers Energy was presented with a unique problem concerning the efficiency associated with the intermediate-pressure turbine section of a General Electric 160 MW reheat steam turbine. The intermediate-pressure turbine section generates approximately 45 MW of the total 160 MW generated. The enthalpy-drop method for calculating efficiency is very sensitive to fluctuation in exhaust steam pressure. For the particular turbine under consideration the sensitivity to pressure fluctuation is exasperated by the physical geometry of the exhaust duct. A pressure correction algorithm was developed using empirical data in conjunction with the fundamental conservation laws.

ACKNOWLEDGEMENTS

I would like to thank my family and friends for their continued and unwavering support. I would like to express my gratitude to my advisor, committee members and corporate mentor respectively, Dr. Engeda, Dr. Mueller, Dr. Shih, and David Hubert, Michigan State University Department of Mechanical Engineering and Consumers Energy for providing me the opportunity to participate in this research project.

TABLE OF CONTENTS

LIST OF TABLES

LIST OF FIGURES

NOCMENCLATURE

Area	A
Control Surface	C.S.
Control Volume	C.V.
Density	ρ
Dynamic Viscosity	μ
Gas Constant	R
Heat Energy	Q
Hydraulic Diameter	d_h
Internal Energy	u
Mass Flow Rate	$\dot{m}$
Radius	r
Rate of change of energy associated with mass flow	$\dot{E}_{mass}$
Rate of change of system energy	$\Delta\dot{E}_{system}$
Reynolds Number	Re_D
Specific Enthalpy	h
Specific Entropy	s
Specific Heat at a constant pressure	C_p
Specific Kinetic Energy Difference Coefficient	β
Specific Kinetic Energy	ke
Specific Potential Energy	pe

Specific Volume	v
Specific Work	w
Stagnation Enthalpy	h_0
Static Pressure	P
Static Temperature	T
Total-to-Total Efficiency	η_{tt}
Velocity	V
Volumetric Flow Rate	$\forall$
Wetted Perimeter	P_w
Work	W

INTRODUCTION

The primary goals for this research project are:

I. Provide a pressure measurement correction algorithm. The pressure measurements are used to calculate turbine efficiency. Currently the measured pressure values do not compensating for the physical geometry of the intermediate-pressure exhaust duct.

II. Additionally, the algorithm must be compatible with the existing test protocol currently employed by Consumers Energy.

The pressure correction algorithm will be used to accurately determine the mechanical work efficiency of an intermediate-pressure (IP) steam turbine section of a General Electric (GE) 3,600 rpm, tandem compound, triple-flow, 160 MW reheat steam turbine with a hydrogen-cooled generator. The design efficiency for the IP turbine internal blading is approximately 91.81%. The efficiency value is based on the available energy in the bowl (inlet) of the IP turbine, and the energy state of the exhaust fluid. The particular turbine under consideration does not have measurement devices located in the bowl section; however, static pressure and temperature measurements are recorded upstream of the intercept valves and downstream of the IP turbine in the crossover duct. The current measurement devices and measurement locations reveal limited information about the energy state of the working fluid. The specific design parameters and specifications are not known due to proprietary concerns. Also, since piping arrangements and a variety of other parameter are subject to

change from one turbine installation to the next, it is difficult for the OEM to provide a standard efficiency value for each system. However, using the available empirical data and accounting for the physical geometry of the exhaust-duct, a sound thermodynamic and fluid mechanic analysis was conducted.

Chapter 1

DESCRIPTION OF VARIOUS STEAM TURBINES

Condensing Steam Turbines

Condensing turbines are the most common type of turbine in the power generation industry. Condensing turbines consist of a steam turbine where main steam is supplied at the most economical pressure and temperature within design parameters. The primary purpose of the condensing turbine is to produce electricity at the most economic cost. This is partially achieved by extracting steam from various stages of the turbine. The extracted steam supplies the feed-water heaters with the energy used to preheat water entering the steam generator.

Non-condensing Steam Turbines

In the strictest sense, the classification of non-condensing turbine includes any turbine where the exhaust steam is not condensed. However, its distinguishing characteristic is that the backpressure is greater than atmospheric pressure. Non-condensing turbines have two primary applications. The first application is in an industrial setting, where process steam is needed that possesses a significant amount of energy. The second application is in the power generation industry where super-positioning of a high-pressure turbines are used to optimize the overall cycle. The exhaust from the high-pressure turbine supplies a low-

pressure turbine. Generally, when this type of arrangement is used it requires significant modifications to the steam generator.

Automatic Extraction Steam Turbines

The classification of automatic extraction turbines includes single, double and triple automatic turbines. Automatic extraction turbines are designed for the extraction of large quantities of process steam.

Mechanical-Drive Units

Mechanical-drive turbines are used to drive other equipment. Large power generation plants commonly use steam turbines to drive boiler feed pumps.

Turbines are also classified by method of control as well.

Throttling Machines

Throttling machines are turbines equipped with a valve in the main steam line. The valve is used to decrease or increase the load on the turbine by adjusting the applied pressure. In terms of economics, the initial investment for this control method is relatively low. The throttling control method is very efficient at full load; however, at intermediate load ranges efficiency is sacrificed. This trend is exasperated at very low load ranges.

Multi-valve Machines

Multi-valve machines are turbines with multiple valves, which distribute the steam flow to various individual nozzle groups in the first stage of the turbine. At lower loads the multi-valve controlled turbine is more efficient, allowing the full pressure force to be applied to the first stage, but decreasing the volumetric flow rate of the steam.

Overload-valve Machines

Turbines with overload-valve arrangement are usually equipped with multiple control valves. These turbines are also equipped with a separate valve in the main steam line, which permits a portion of the main steam to flow to a lower stage in the turbine; this stage is referred to as the "overload stage". The overload stage pressure approaches line pressure, increasing the flow through the turbine. Typically all the main steam is forced through the first stage, where the effective cross-sectional area is limited, but by routing some of the main steam to the overload stage where the effective cross-sectional area is greater efficiency is improved at lower loads without sacrificing efficiency at higher loads.

Stage-valve Machines

The stage-valve is similar to the overload-valve; the primary difference is the stage-valve extracts the steam after the steam exits the first stage. The steam exiting the first stage has a reduced temperature. The cooler steam is usually routed to the third or fourth stage. The primary purpose of the stage bypass is to

prevent the first-stage shell pressure from increasing to the point where the main steam pressure becomes restrictive.

Figure 1 illustrates the various valve configurations.

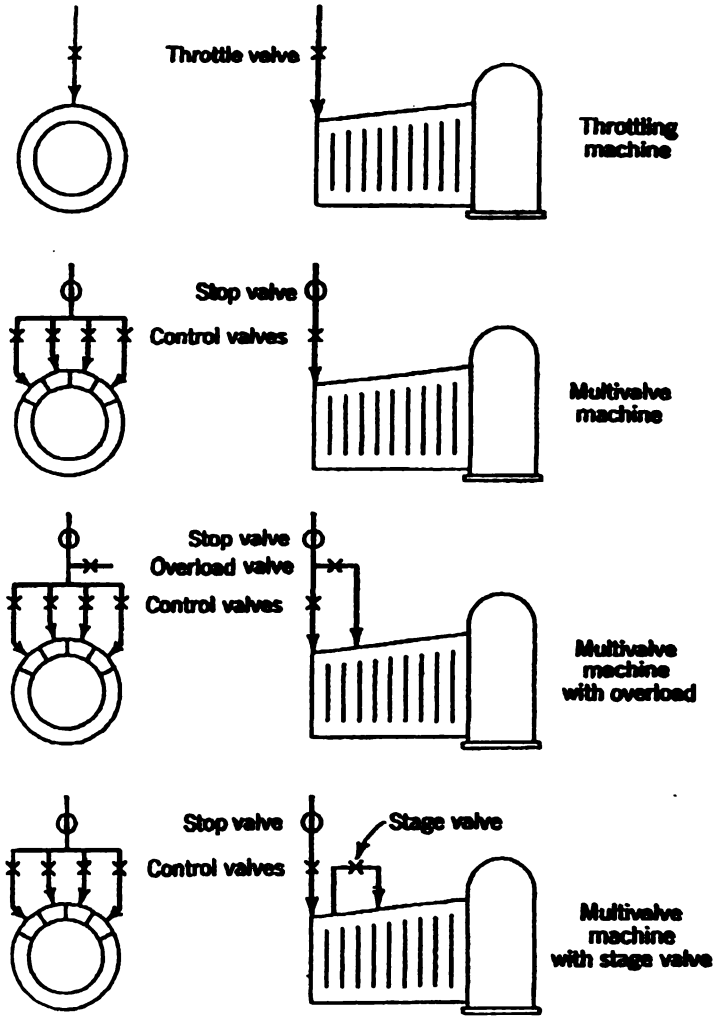

Figure 1: Various control valve arrangements.

LITERATURE REVIEW

Section 4 of the AMSE PC 6-1976 performance test code, discusses Instruments and Methods of Measurement. Sub-section 4.56 lists the criteria for the enthalpy-drop method for determining steam turbine efficiency. The most important criterion is the type of steam turbine this test is applicable for. The performance code states the enthalpy-drop test is suitable for non-condensing turbines or backpressure turbines with a minimum mass flow rate of $50{,}000\frac{lb_m}{hr.}$, and an exhaust temperature of at least 27 °F. Additionally, sub-section 4.56 states no less than two independent determinations of inlet enthalpy and of exhaust enthalpy shall be made. The Measurement of Pressures section reinforces this, and more specifically sub-section 4.90, which discusses initial-pressure measurements and sub-section 4.92 that covers exhaust pressure measurements. The term initial-pressure measurement refers to the pressure at the inlet of the turbine under consideration. Section 4.90 dictates that the pressure measurements are recorded upstream of the intercept valves of the IP turbine, this is the location where the empirical data was collected for the efficiency analysis. Sub-section 4.92 requires the installation of a pressure measurement device for every sixteen square feet of cross-sectional area, but sub-section 4.56 requires a minimum of two measurement devices. The cross-sectional area of the exhaust duct under consideration is twenty-five square feet; therefore, either case requires at least two pressure measurement devices for the exhaust fluid. The empirical data collected for this analysis is the average of

two different exhaust-pressure measurement devices. However, there is concern about the location of the exhaust pressure measurement devices. According to sub-section 4.93 the pressure measurement devices ideally should be located where the exhaust duct connects to the expansion joint; this section is shown in figure 2.

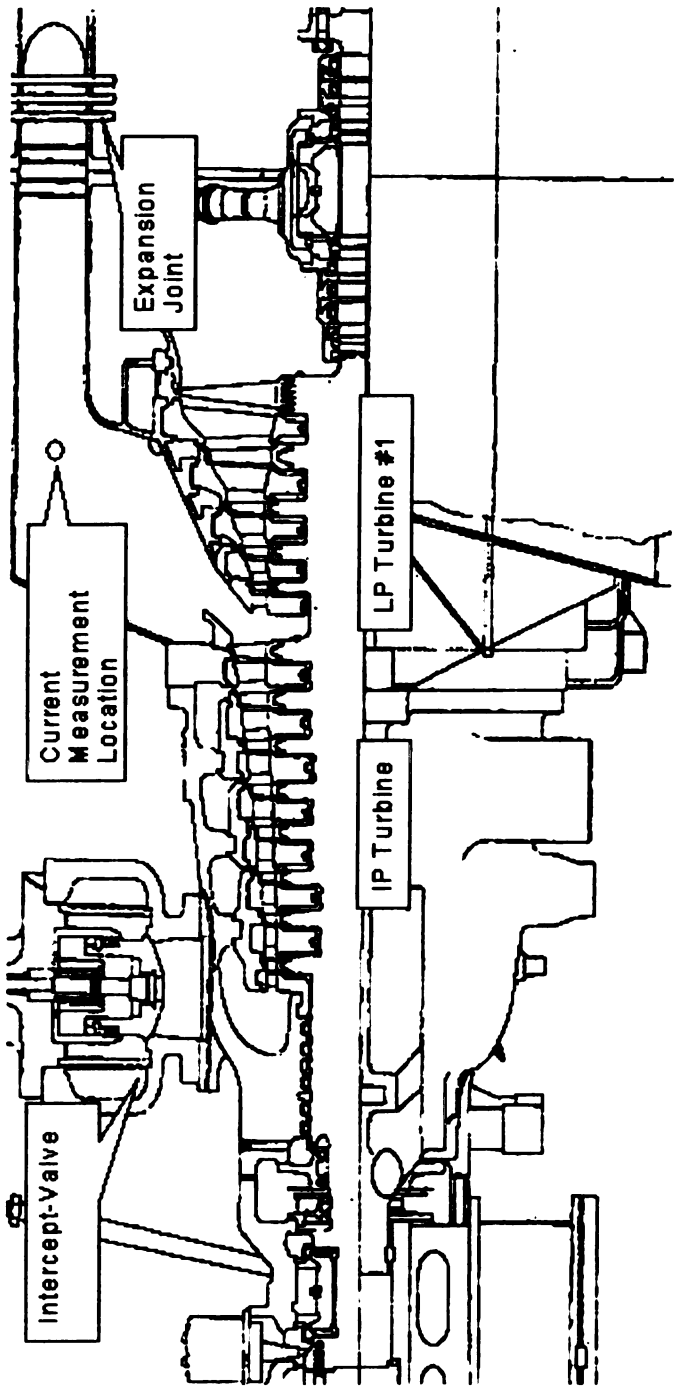

Figure 2: Intermediate-pressure turbine cross-section.

The portion of section 4, which covers the Measurement of Temperatures, discusses optimal locations for temperature measurement devices. Sub-section 4.102 states that temperature devices used for measuring temperatures pertaining to enthalpy drops should be located very close to the corresponding pressure measurement device. Sub-section 4.103 states that, if the temperature measurement is an influential measurement (which is the case for the enthalpy-drop test) the measurement device should be located immediately downstream of a pipe elbow. The flow separation associated with the change in direction of the flow induces turbulence; thereby, mixing the fluid which yields a more accurate mean-temperature measurement.

The location of the measurement devices coincides with the ASME performance test code for the most part; however, a few changes should be implemented regarding the location of the exhaust measurement devices. Additionally, the number of devices in the exhaust duct should be increased so a more precise interpretation of the flow field can be determined. ASME is the leading authority on performance testing of steam turbines and is also the industry standard; therefore, the ASME performance test codes was used as the benchmark and the primary source of information used for this study.

Chapter 2

TURBINE EFFICIENCY ANALYSIS

Figure 3 illustrates the defined control volume and surfaces:

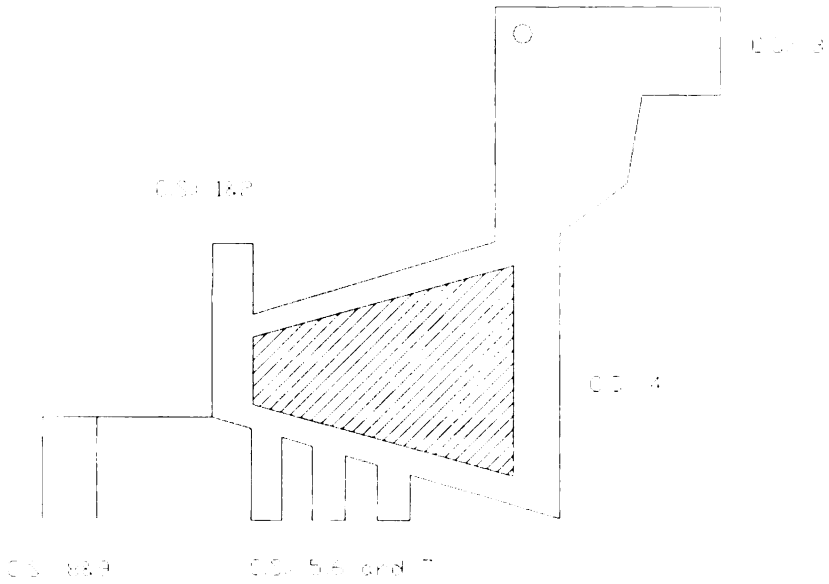

Figure 3: Control volume and control surfaces.

The following assumption were invoked for the turbine efficiency analysis:

1. Cartesian coordinate system: (x, y, z)
2. Steady-state: $\frac{\partial}{\partial t} = 0$
3. Adiabatic process: $\Delta Q = 0$
4. Ideal gas: $P = \rho RT$

Conservation of Mass:

There are no mass sinks or sources in the control volume, therefore mass is conserved. The integral form of the conservation of mass was employed as the governing equation for continuity.

$$\frac{D(M_{sys})}{Dt} = \frac{\partial}{\partial t}\int_{cv}\rho d\forall + \int_{cs}\rho(\bar{V}\cdot\hat{n})dA; \quad M_{sys} = \int_{sys}\rho d\forall$$

Equation 1: Conservation of mass.

Since the mass of the system is not a function of time its derivative with respect to time is zero:

$$\frac{D(M_{sys})}{Dt} = 0$$

The steady-state assumption reduces the conservation of mass equation to:

$$0 = \int_{cs}\rho(\bar{V}\cdot\hat{n})dA = \sum_{cs1}^{cs9}\int\rho(\bar{V}\cdot\hat{n})dA$$

The differential cross-sectional area for a circular duct is:

$$dA = 2\pi r dr$$

The differential cross-sectional area for a rectangular duct:

$$dA = dxdy$$

The resulting equation is:

$$0 = -\int_0^R \rho_1 V_1 2\pi r dr - \int_0^R \rho_2 V_2 2\pi r dr + \int_{y1}^{y2}\int_{x1}^{x2}\rho_3 V_3 dxdy + \int_0^R \rho_4 V_4 2\pi r dr + \int_0^R \rho_5 V_5 2\pi r dr +$$
$$\int_0^R \rho_6 V_6 2\pi r dr + \int_0^R \rho_7 V_7 2\pi r dr + \int_0^R \rho_8 V_8 2\pi r dr + \int_0^R \rho_9 V_9 2\pi r dr$$

Once integrated, each integral is equal to:

$$\dot{m}_? = \rho_? V_? A_?$$

Control surfaces 1 and 2 have the same mass flow rate, this is due to the geometric symmetry of both control surfaces; furthermore, control surface 1 and 2 is where the steam enters the IP Turbine. It is assumed that the mass flow is evenly divided between the control surfaces,

$$\dot{m}_1 + \dot{m}_2 = \dot{m}_1 + \dot{m}_1 = 2\dot{m}_1 = \dot{m}_{in}$$

The mass balance is:

$$\dot{m}_{in} = \dot{m}_3 + \dot{m}_4 + \dot{m}_5 + \dot{m}_6 + \dot{m}_7 + \dot{m}_8 + \dot{m}_9$$

Out of the nine control surfaces identified, the mass flow rates are known for seven of the nine. The mass flow rates for control surfaces 3 and 4 are unknown. Static pressure and temperature measurements are recorded at control surface 3; however, neither thermodynamic properties nor mass flow measurements are known at control surface 4. It is assumed that (2/3) of the mass downstream of the last steam extraction exits through control surface 3, and the additional (1/3) exits through control surface 4. This assumption was adopted because the mass that exits through control surface 3 exhausts to the double-flow low-pressure (LP) turbine. The mass that exits through control surface 4 exhausts to the single flow LP turbine. Each LP turbine was designed to operate at the same volumetric flow rate and thermodynamic state; therefore, (2/3) of the working fluid exhausts through control surface 3 and (1/3) exhausts through control surface 4; additionally, the thermodynamic properties for control surface 3 will be applied at control surface 4.

The mass flow rates for control surfaces 3 and 4 can be expressed as:

$$\dot{m}_3 = \frac{2}{3}(\dot{m}_{in} - \dot{m}_5 - \dot{m}_6 - \dot{m}_7 - \dot{m}_8 - \dot{m}_9) = \frac{2}{3}(\dot{m}_x)$$

$$\dot{m}_4 = \frac{1}{3}(\dot{m}_{in} - \dot{m}_5 - \dot{m}_6 - \dot{m}_7 - \dot{m}_8 - \dot{m}_9) = \frac{1}{3}(\dot{m}_x)$$

Combining the two previous expressions, the result is:

$$\dot{m}_{in} = \frac{2}{3}\dot{m}_x + \frac{1}{3}\dot{m}_x + \dot{m}_5 + \dot{m}_6 + \dot{m}_7 + \dot{m}_8 + \dot{m}_9$$

$$\frac{2}{3}\dot{m}_x + \frac{1}{3}\dot{m}_x = \dot{m}_{in} - \dot{m}_5 - \dot{m}_6 - \dot{m}_7 - \dot{m}_8 - \dot{m}_9$$

where,

$$\dot{m}_x = \dot{m}_{in} - \dot{m}_5 - \dot{m}_6 - \dot{m}_7 - \dot{m}_8 - \dot{m}_9$$

The calculation of $\dot{m}_x$ is listed below:

Control surface 1:

$$\dot{m}_1 = 433{,}060\frac{lb_m}{hr} = 120.294\frac{lb_m}{s}$$

$$P_1 = 358.6 psia$$

$$T_1 = 959.5\,°F$$

$$h_1 = 1503.41\frac{Btu}{lb_m}$$

Control surface 2:

$$\dot{m}_2 = 433{,}060 \frac{lb_m}{hr} = 120.294 \frac{lb_m}{s}$$

$$P_2 = 358.6 psia$$

$$T_2 = 959.5\,^{\circ}F$$

$$h_2 = 1503.41 \frac{Btu}{lb_m}$$

Control surface 3:

$$\dot{m}_3 = \frac{2}{3}\dot{m}_x$$

$$P_3 = 36.3 psia$$

$$T_3 = 416.1\,^{\circ}F$$

$$h_3 = 1245.81 \frac{Btu}{lb_m}$$

Control surface 4:

$$\dot{m}_4 = \frac{1}{3}\dot{m}_x$$

$$P_4 = 36.3 psia$$

$$T_4 = 416.1\,^{\circ}F$$

$$h_4 = 1245.81 \frac{Btu}{lb_m}$$

Control surface 5:

$$\dot{m}_5 = 47{,}180\frac{lb_m}{hr} = 13.1056\frac{lb_m}{s}$$

$$P_5 = 53.5 psia$$

$$h_5 = 1300.5\frac{Btu}{lb_m}$$

Control surface 6:

$$\dot{m}_6 = 22{,}490\frac{lb_m}{hr} = 6.247\frac{lb_m}{s}$$

$$P_6 = 106 psia$$

$$h_6 = 1368\frac{Btu}{lb_m}$$

Control surface 7:

$$\dot{m}_7 = 37{,}380\frac{lb_m}{hr} = 10.383\frac{lb_m}{s}$$

$$P_7 = 189 psia$$

$$h_7 = 1482\frac{Btu}{lb_m}$$

Control surface 8:

$$\dot{m}_8 = 2{,}950\frac{lb_m}{hr} = 0.8194\frac{lb_m}{s}$$

$$P_8 = ? psia$$

$$h_8 = 1492.5 \frac{Btu}{lb_m}$$

Control surface 9:

$$\dot{m}_9 = 2{,}650 \frac{lb_m}{hr} = 0.7361 \frac{lb_m}{s}$$

$$P_9 = ?psia$$

$$h_9 = 1492.5 \frac{Btu}{lb_m}$$

The calculated values for $\dot{m}_x, \dot{m}_3$, and $\dot{m}_4$ are,

$$\dot{m}_x = 753{,}470 \frac{lb_m}{hr} = 209.297 \frac{lb_m}{s}$$

$$\dot{m}_3 = \frac{2}{3}\dot{m}_x = 502{,}313.33 \frac{lb_m}{hr} = 139.53 \frac{lb_m}{s}$$

$$\dot{m}_4 = \frac{1}{3}\dot{m}_x = 251{,}156.67 \frac{lb_m}{hr} = 69.77 \frac{lb_m}{s}$$

Substituting in known and calculated mass flow rate values, it was determined mass is conserved.

$$\dot{m}_{in} = \dot{m}_{out}$$

First Law of Thermodynamics:

Since mass conservation of the control volume has been established, a first law analysis will now be conducted.

$$\dot{Q}_{net} + \dot{W}_{net} + \dot{E}mass_{net} = \Delta\dot{E}_{system}$$

Equation 2: First law of thermodynamics.

Expanding equation 2 yields:

$$\dot{Q}_{in} - \dot{Q}_{out} + \dot{W}_{in} - \dot{W}_{out} + \dot{m}_{in}(u + Pv + ke + pe) - \dot{m}_{out}(u + Pv + ke + pe) = \dot{m}_{system}\Delta u$$

Applying the adiabatic and steady state assumptions as well as, assuming the potential energy is negligible; equation 2 can be reduced even further,

$$-\dot{W}_{out} + \dot{m}_{in}(u + Pv + ke) - \dot{m}_{out}(u + Pv + ke) = 0$$

Specific work output is,

$$w_{out} = (h_{0in} - h_{0out})$$

Mechanical work efficiency is,

$$\eta_{tt} = \frac{w_{actual} = w_{out,a} = (h_{01} - h_{03a})}{w_{isentropic} = w_{out,s} = (h_{01} - h_{03s})}$$

Equation 3: Total-to-total efficiency.

To calculate the mechanical efficiency it is necessary to compute the isentropic work. Two independent intensive properties are necessary to thermodynamically fix a state. The two properties used to fix the isentropic state were s_{3s} and P_{2a}, where $s_{in} = s_{3s}$ and $P_{3s} = P_{2a}$. Once the state was thermodynamically fixed the remaining thermodynamic properties were calculated. Total-to-total mechanical

work efficiency takes the kinetic energy of the working fluid into account as well as the internal and flow energy; therefore, the velocities must also be determined. The thermodynamic states have been determined, and the geometry of the control surfaces are known the velocity associated with the mass flux through the control surfaces can be computed, thereby the stagnation enthalpy can be calculated, permitting the determination of the mechanical efficiency.

Stagnation enthalpy at control surface 1 & 2:

$$\dot{m}_{in} = \rho_{in} V_{in} A_{in}$$

$$\dot{m}_{in} = 866{,}120 \frac{lb_m}{hr} = 240.79 \frac{lb_m}{s}$$

$$V_{in} = \frac{\dot{m}_{in}}{\rho_{in} A_{in}} = 39.45 \frac{ft.}{s}$$

$$h_{in} = 1503.41 \frac{Btu}{lb_m} = 37{,}640{,}876.17 \frac{ft.}{s}$$

$$h_{0in} = h_{in} + ke = h_{in} + \frac{V_{in}^2}{2} = 37{,}641{,}645.32 \frac{ft^2}{s^2}$$

Actual stagnation enthalpy at control surface 3_a:

$$\dot{m}_{3a} = \rho_{3a} V_{3a} A_{3a}$$

$$\dot{m}_{3a} = 502{,}313.33 \frac{lb_m}{hr} = 139.53 \frac{lb_m}{s}$$

$$V_{3a} = \frac{\dot{m}_{3a}}{\rho_{3a} A_{3a}} = 227.97 \frac{ft.}{s}$$

$$h_{3a} = 1244.81 \frac{Btu}{lb_m} = 31{,}166{,}307.97 \frac{ft^2}{s^2}$$

$$h_{03a} = h_{in} + ke = h_{in} + \frac{V_{in}^2}{2} = 31{,}192{,}293.13\frac{ft^2}{s^2}$$

Isentropic stagnation enthalpy at control surface 3_s:

$$\dot{m}_{3s} = \rho_{3s} V_{3s} A_{3s}$$

$$\dot{m}_{3s} = 502{,}313.33\frac{lb_m}{hr} = 139.53\frac{lb_m}{s}$$

$$V_{3s} = \frac{\dot{m}_{3s}}{\rho_{3s} A_{3s}} = 218.36\frac{ft.}{s}$$

$$h_{3s} = 1227.80\frac{Btu}{lb_m} = 30{,}740{,}428.60\frac{ft^2}{s^2}$$

$$h_{03s} = h_{in} + ke = h_{in} + \frac{V_{in}^2}{2} = 30{,}764{,}269.15\frac{ft^2}{s^2}$$

The total-to-total mechanical work efficiency for the defined control volume is,

$$\eta_{tt} = \frac{w_{actual} = w_{out,a} = (h_{01} - h_{03a})}{w_{isentropic} = w_{out,s} = (h_{01} - h_{03s})} = 93.80\%$$

The calculated efficiency is higher than the estimated design efficiency. This result is most likely due to the pressure value measured in the crossover duct, because of the turbulent nature of the exhaust flow and the rectangular geometry of the duct a correction is necessary to achieve an accurate efficiency value, which will be discussed in the next chapter. Figure 4 and 5 illustrate the expansion process through the intermediate-pressure turbine.

Images in this thesis are presented in color.

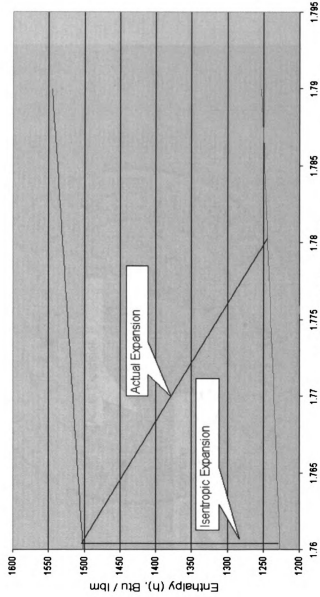

Figure 4: Enthalpy vs. entropy diagram.

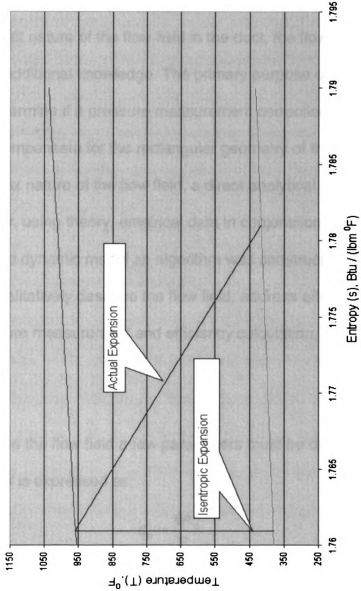

Figure 5: Temperature vs. entropy diagram.

Chapter 3

PRESSURE CORRECTION ANALYSIS

Due to the turbulent nature of the flow field in the duct, the flow field cannot be resolved without additional knowledge. The primary purpose of this research project was to determine if a pressure measurement correction algorithm could be produced to compensate for the rectangular geometry of the crossover duct. Due to the complex nature of the flow field, a direct analytical solution is not possible. However, using theory, empirical data in conjunction with a computational fluid dynamic model an algorithm was constructed. The following discussion will qualitatively describe the flow field, address effects of the flow field on the pressure measurement and efficiency calculation, and discuss algorithm results.

In order to describe the flow field a few parameters must be defined. The hydraulic diameter is expressed as,

$$d_h = \frac{4A_c}{P_w}$$

This characteristic length scale is a ratio of the area to the wetted perimeter; it was derived so that the geometric diameter of a circular duct is equal to the hydraulic diameter. The hydraulic diameter of the crossover duct is,

$$d_h(x) = \frac{20}{11}$$

Using the hydraulic diameter as the characteristic length to evaluate the Reynolds number the result is,

$$Re_D = \frac{\rho V d_h}{\mu} = 2.91 \times 10^6$$

The order of magnitude of the Reynolds number indicates the flow is turbulent. Inertial forces dominate turbulent flows, as apposed to laminar flows, which are dominated, by viscous forces. Additionally, the unsteady nature of turbulent flow makes exact analytical solutions nearly impossible. The power-law velocity profile approximation is a function derived from empirical data:

$$\frac{w}{V_c} = \left(1 - \frac{r}{R}\right)^{\frac{1}{n}}$$

The power-law approximates the velocity profile for some fully developed turbulent flows. The variable n is a function of the Reynolds number. The domain of the n-function is, $10^4 < Re_D < 10^7$, the resulting range is $5 \le n \le 11$. The power-law is the turbulent analog of Poiseuille flow for laminar flow conditions. The primary assumption for both Poiseuille flow and the power-law approximation is the fully developed assumption. The distance required for the forces acting on a fluid element to become balanced is referred to as the entrance length,

$$\frac{l_e}{d_h} = 4.4(Re_D)^{\frac{1}{6}}$$

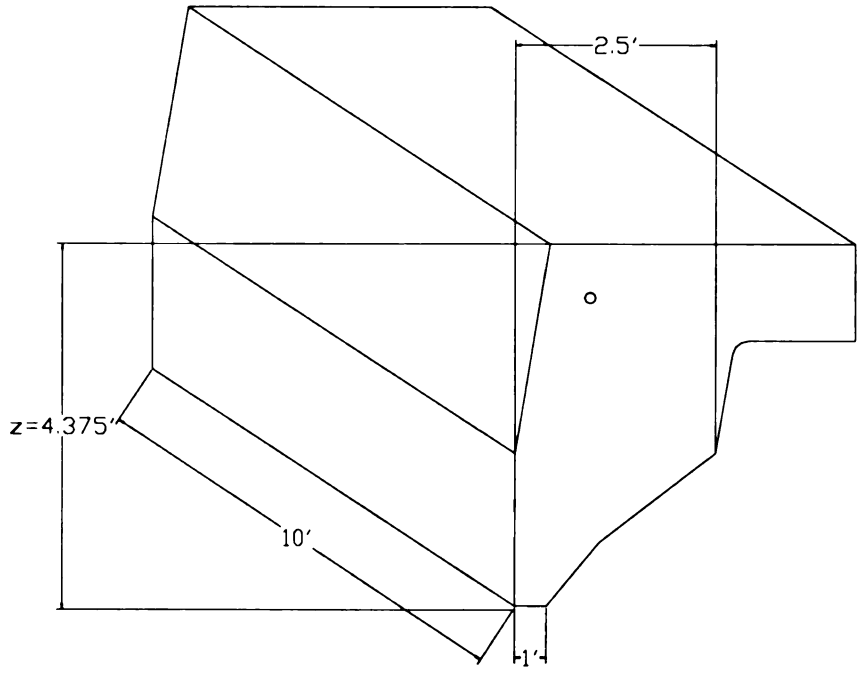

Figure 6: Control volume.

The entrance length required for the previously calculated Reynolds number is $l_e = 95.59\,\text{ft.}$, and z=4.375 ft., as illustrated by the figure 2. Scaling the height of the duct to the entrance length yields the following expression,

$$\frac{z = 4.375\,\text{ft.}}{l_e = 95.59\,\text{ft.}} = 0.045768$$

The fully developed assumption dictates that this ratio assumes values greater than one,

$$\frac{z}{l_e} > 1$$

The vertical distance from the entrance of the duct to the location of the pressure transducer is much less than the length required for the fully developed flow

assumption. The entrance length required for turbulent flows is considerably greater than the entrance length required for laminar flows.

The ratio of the hydraulic diameter to the height is:

$$\frac{z = 4.375\,\text{ft.}}{d_h = 1.82\,\text{ft.}} = 2.41$$

Poiseuille flow and the power-law approximation are used to determine the pressure drop of a flow over some finite length; however, the length is usually many times greater than the hydraulic diameter of the duct.

To determine the impact of compressibility effects on the flow, the Mach number was also computed:

$$Ma = \frac{V = 228\,\frac{\text{ft.}}{\text{s}}}{a = 1767\,\frac{\text{ft.}}{\text{s}}} = 0.129$$

V is the average velocity and "a" is the speed of sound. As a rule of thumb for values of the Mach number less than 0.3, compressibility effects are negligible.

During the search for an analytical solution, all the conservation laws were applied to the defined control volume; the momentum balance, nor the conservation of energy were able to account for the pressure drop directly. Examining and manipulating the empirical data collected a pattern was detected in the pressure values. The measured pressure yields an efficiency of approximately 93.8%, an average increase of 2% greater than design efficiency.

The 2% increase in efficiency is directly associated with an average 2 psia increase in pressure.

For most practical engineering problems, a discrepancy of 2 psia is negligible; however, turbine efficiency is very sensitive to discharge pressure values. From the energy equation the pressure difference can be expressed in terms of potential and kinetic energy. Since the pressure transducer is mounted horizontally the body force associated with gravity is neglected. The pressure difference expressed in terms of a kinetic energy difference is:

$$\Delta P = 2psia = \frac{1}{2}\rho\left(V_2^2 - V_1^2\right) = \frac{1}{2}\rho\left(\Delta V^2\right) = 9{,}273.6\frac{lbm}{ft.s^2}$$

Physically, the previous expression represents the volumetric kinetic energy difference. Re-expressing the volumetric kinetic energy term as a specific kinetic energy difference term gives the following expression

$$\frac{\Delta V^2}{2} = 131{,}710\frac{ft.^2}{s^2} = 5.26\frac{Btu}{lbm}$$

The magnitude of the specific kinetic energy difference term may seem small; however, considering that sub-regions in the flow are in relatively close proximity, the change in energy is a fairly dramatic.

It will be verified later in the discussion that the static temperature is fairly constant throughout the flow field, therefore assuming static temperature is constant the enthalpy difference associated with the differential pressure is:

$$\Delta h = 1245.07 - 1244.81 = 0.256252 \frac{Btu}{lbm} = 6{,}409.5 \frac{ft.^2}{s^2}$$

The entropy difference for calorically perfect gases is,

$$s_2 - s_1 = c_p \ln \frac{T_2}{T_1} - R \ln \frac{p_2}{p_1}$$

The equation indicates that if the temperature is constant, the entropy difference is only a function of pressure. The underline physical significance is the internal energy of the fluid is constant; however, the flow energy does vary from region to region, inducing losses. These losses are more commonly associated with the Reynolds stress terms,

$$\tau_{turb} = \rho \overline{u' v'}$$

This further supports the concept that shear stresses induced by inertial forces dominant turbulent flows. The ratio of the enthalpy change to the change is kinetic energy from the high-pressure region to the low-pressure region is,

$$\frac{\frac{\Delta V^2}{2}}{\Delta h} = \frac{5.26 \frac{Btu}{lbm}}{0.256 \frac{Btu}{lbm}} = 20.527$$

Numeric methods are not the primary scope of this research project; however, a computational fluid dynamic model was created of the geometry, in order to help visualize the physics of the flow. Using the information provided by the model in conjunction with the empirical data an algorithm will be created to account for the pressure measurement discrepancy.

Assumptions for the computational fluid dynamic model are:

1. Uniform inlet velocity profile
2. Pressure outlet
3. Reynolds stress turbulent model
4. Working fluid: Air
5. No slip boundary condition
6. Unstructured mesh

The pressure transducer is located in the region of high pressure indicated by the orange contour lines on figure 7; 2.49E+5 Pascal are equivalent to 36.1 psia, approximately the same value measured by the pressure transducer.

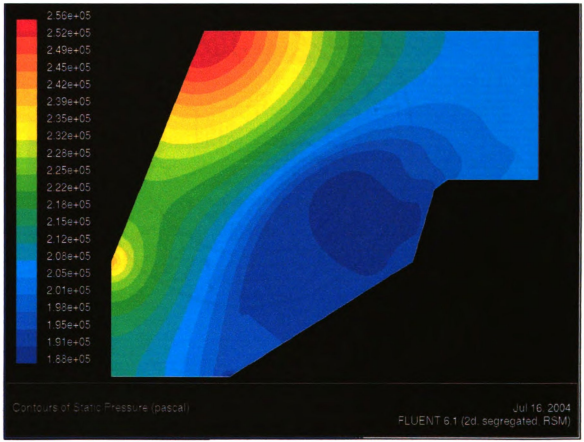

Figure 7: Contours of static pressure.

Moving toward the center of the flow the pressure drops even further. The pressure values associated with the darker blue regions are relatively low because of the existence of a forced or rotational vortex in that region. Initial at start-up when the steam first starts to flow, separation occurs in the duct section because of the rapid change in the duct geometry. As the turbine reaches steady state conditions mass from the bulk flow will no longer be transferred to the vortex. The angular velocity of the forced vortex is maintained via momentum transfer through the shear layer from the bulk flow to the vortex.

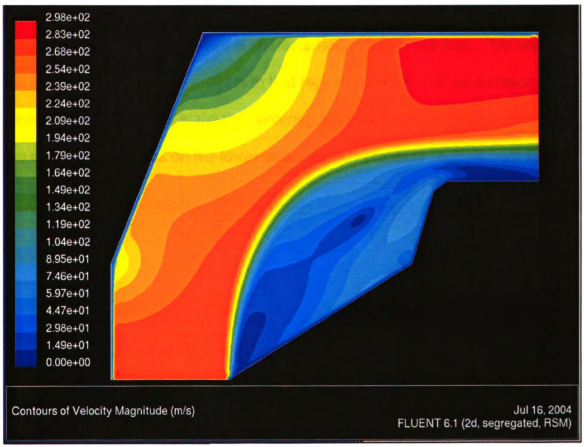

Figure 8: Contours of velocity magnitude.

Flow separation alters the aerodynamic geometry of the flow field. In the case of an air foil the geometry change results in a reduction in lifting capacity, in the case of a diffuser the pressure recovery is minimized and diffuser efficiency is compromised. For this situation the geometric change reduces the effective cross-sectional area; thereby, accelerating the fluid through the turn. This is demonstrated in figure 8.

The previous points will be fundamental in the logic behind the algorithm. The velocity contours reveal that different regions of the flow field posses varying amounts of kinetic energy. The blue region has sections where the velocity magnitude is zero; this behavior is characteristic of forced vortices. This supports the idea that a forced vortex exists in that region. An additional observation about figure 8 that is important is the fluid entering the duct is forced to the center by the shape of the vortex on the lower side and high-pressure regions from above.

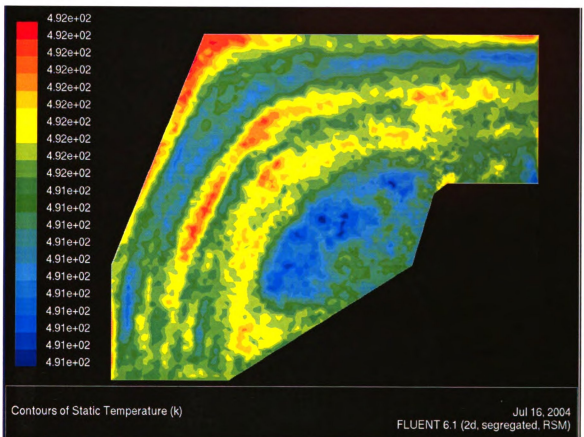

Figure 9: Contours of static temperature.

The thermal couples seem to provide accurate temperature readings; Figure 9 provides insight on why. Except for stagnate regions (indicated with red) and the region containing the vortex the temperature distribution is constant for the most part, this can be attributed to the adiabatic boundary condition. Since the thermal energy is not transferred to the surroundings, it permeates the flow field; this results in a nearly even temperature distribution.

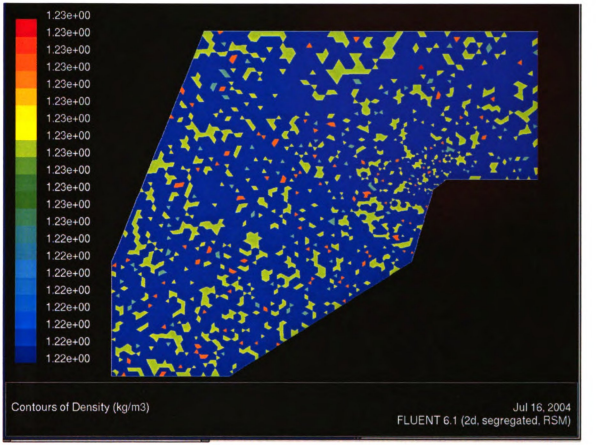

Figure 10: Contours of density.

Continuous momentum transfer between regions induces a mixing effect, which is demonstrated by figure 10. This mixing action results in a fairly even density distribution over the flow field.

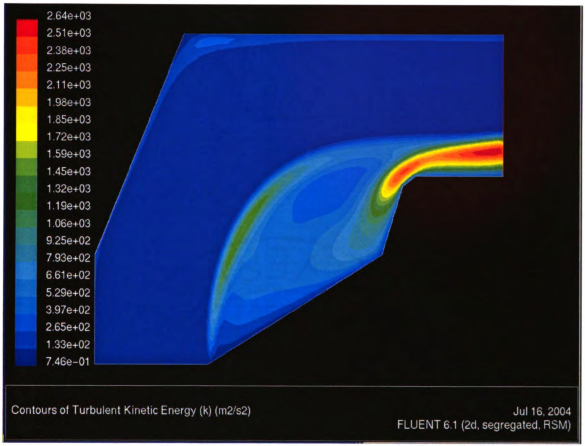

Figure 11: Contours of turbulent kinetic energy.

Figure 11 reveals that the bulk of the turbulent energy is confined to the vortex. Figure 11 also suggests that the darker blue region is nearly void of turbulent kinetic energy; however, because the model is two-dimensional it is not capturing the turbulent effects of the third dimension.

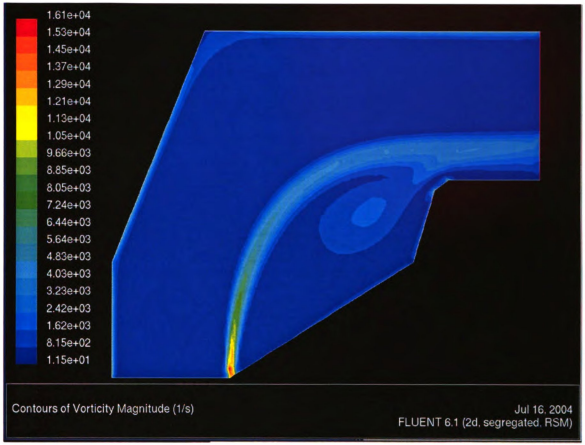

Figure 12: Contours of the vorticity magnitude.

From figure 12 it can be seen that the vorticity magnitude (the curl of the velocity vector) has the largest value at the inlet where the shear layer is first created between the main flow field, and the clock-wise rotation of the forced vortex. Figure 12 also indicates that the fluid near the inlet where the two flow fields intersect has behavior characteristic of an irrotational vortex where the velocity near the center approaches infinity.

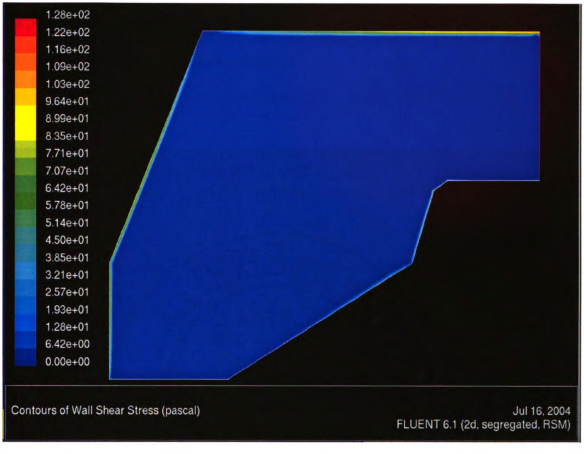

Figure 13: Contours of wall shear stress.

Figure 13 illustrates, that for turbulent flows the viscous effects are confined to a very small region near the surface.

The enthalpy contours resemble the static temperature contours, this is no surprise since superheated steam behaves similarly to an ideal gas, and ideal gases are functions of temperature only.

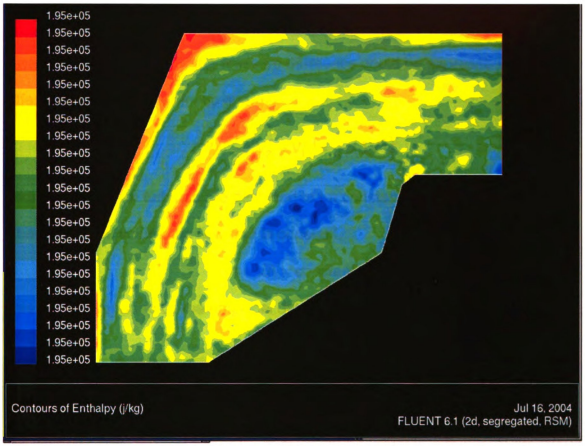

Figure 14: Contours of enthalpy.

The following discussion will explain the underlying concepts of the pressure correction algorithm. In order to account for the pressure difference, knowledge of the flow field inside the duct and the corresponding boundary conditions are necessary. Only one pressure boundary condition is known and nothing is known

about the velocity profile or pressure distribution inside the duct. Additionally, the flow is under developed turbulent flow. However, upon further investigation using some design characteristics about the turbine, employing some physics and the use of a computational fluid dynamic model a pressure correction algorithm was produced

It was discussed earlier that a pressure difference could be expressed as a difference in volumetric kinetic energy,

$$\Delta P = \frac{1}{2}\rho\left(V_2^2 - V_1^2\right) = \frac{1}{2}\rho\left(\Delta V^2\right)$$

Additionally, steam turbines are designed to be constant volume machines, in other words the volumetric flow rate is constant,

$$\forall = VA = \text{constant}$$

This fact is supported by the empirical data collected, which is displayed in table 1.

Uncorrected Efficiency Values								
		Inlet Conditions			Exhaust Conditions			
MW	m, (lb_m/hr)	vol. flow ($ft.^3$/hr)	P_1, (psia)	T_1, (^0F)	P_2, (psia)	T_2, (^0F)	η	P_1/P_2
158	876,105.00	2,015,194.63	363.8	969.8	36.9	423	93.87%	9.86
155	866,750.00	2,007,488.43	358.6	959.5	36.3	416	93.82%	9.88
150	838,488.00	2,006,408.51	346.7	957.2	34.5	411.2	93.85%	10.05
147	817,173.00	2,005,103.45	337.8	955.4	33.7	409.9	93.96%	10.02
144	801,959.00	2,002,822.74	331.1	951.8	33	407.8	93.89%	10.03
142	775,638.00	2,018,522.40	322.7	971.9	32.2	419.1	94.34%	10.02
138	745,183.00	2,030,035.29	311.7	986.2	31.3	432.5	93.93%	9.96
135	726,709.00	2,025,846.92	304.7	986.2	30.7	433.6	93.87%	9.93
134	708,901.00	2,038,577.34	297.8	997	29.9	440.2	93.90%	9.96
131	690,681.00	2,038,452.13	290.2	996.7	29.2	440.8	93.85%	9.94
127	668,339.00	2,042,343.44	281.3	1001.2	28.1	442.5	93.86%	10.01
123	649,383.00	2,042,178.76	273.4	1001	27.3	442.7	93.81%	10.01
120	633,679.00	2,042,540.44	266.8	1000.9	26.7	442.7	93.88%	9.99
116	609,838.00	2,039,404.62	256.3	995.6	25.7	440.5	93.72%	9.97
113	595,370.00	2,038,601.24	250.1	994	25.1	439.3	93.78%	9.96
110	576,145.00	2,037,616.61	241.9	992.1	24.3	438.4	93.76%	9.95
106	558,694.00	2,028,343.21	233.6	979.5	23.5	431.6	93.52%	9.94
103	550,544.00	2,016,424.77	228.8	962.8	23	420.2	93.51%	9.95
100	529,375.00	2,020,263.32	220.4	967.3	22.2	421	93.97%	9.93
97	511,847.00	2,026,661.14	213.8	975.7	21.6	427.5	93.95%	9.90

Table 1:Empirical data.

The volume flow varies by a margin of approximately 30,000 cubic feet per hour, but this is negligible compared to 2,000,000 cubic feet per hour, which is the average flow rate; therefore, constant volumetric flow rate is a reasonable approximation.

Using the empirical data the discharge pressure was adjusted until the correct efficiency values were achieved, this is demonstrated in table 2.

Corrected Efficiency Values					
vol. flow ($ft.^3/hr$)	P_2, corr. (psia)	T2, (^0F)	η, corr.	P_1/P_2, corr. (psia)	P_2-P_2, corr. (psia)
2,015,194.63	34.59	423	91.81%	10.52	2.313
2,007,488.43	34.09	416	91.81%	10.52	2.21
2,006,408.51	32.34	411.2	91.81%	10.72	2.16
2,005,103.45	31.48	409.9	91.81%	10.73	2.22
2,002,822.74	30.90	407.8	91.81%	10.72	2.1
2,018,522.40	29.71	419.1	91.81%	10.86	2.49
2,030,035.29	29.26	432.5	91.81%	10.65	2.04
2,025,846.92	28.76	433.6	91.81%	10.59	1.94
2,038,577.34	27.97	440.2	91.81%	10.65	1.93
2,038,452.13	27.36	440.8	91.81%	10.61	1.84
2,042,343.44	26.31	442.5	91.81%	10.69	1.79
2,042,178.76	25.61	442.7	91.81%	10.68	1.695
2,042,540.44	24.99	442.7	91.81%	10.68	1.715
2,039,404.62	24.17	440.5	91.81%	10.60	1.53
2,038,601.24	23.56	439.3	91.81%	10.62	1.54
2,037,616.61	22.82	438.4	91.81%	10.60	1.476
2,028,343.21	22.25	431.6	91.81%	10.50	1.254
2,016,424.77	21.78	420.2	91.81%	10.51	1.22
2,020,263.32	20.71	421	91.81%	10.64	1.49
2,026,661.14	20.17	427.5	91.81%	10.60	1.435

Table 2: Manipulated empirical data.

The result of this exercise revealed that the average difference in pressure between the measured values and the theoretical values is 1.82 psia. Additionally, the data shows that as the mass flow rate decreases the pressure difference decreases. The reduction in the pressure difference is due to the decrease in density as the mass flow rate decreases; however, the volume flow rate is constant as show in figure 15.

Figure 15: Mass flow rate vs. density.

Using this fact even though the complex aerodynamic geometry is not known, what is known is the kinetic energy in the duct is constant over the load range. If the volume flow rate is a constant,

$$\forall = VA = \text{constant}$$

The area of the turbine is constant therefore the velocity must be constant. This should be interpreted as the velocity may differ from one point to another point in the flow, but at any given point the velocity is constant. This is also validated by the steady-state assumption. Although the flow field is not functionally defined, there is an imaginary location associated with the difference in kinetic energy. Since the pressure difference is equivalent to a volumetric kinetic energy difference, and it has been established that the velocity at any given point in the flow is constant then the specific kinetic energy difference is constant,

$$\frac{\Delta P}{\rho} = \frac{\Delta\left(V_2^2 - V_1^2\right)}{2} = \frac{\Delta\left(V^2\right)}{2} = \Delta ke = \text{constant}$$

The pressure difference becomes a function of density. At this point two pieces of information are necessary to proceed with the algorithm, a determination of the specific kinetic energy and a density value. The determination of the density can be made from the measured pressure and temperature values. It is assumed that the density distribution is fairly constant, this due to the turbulent nature of the flow, and is demonstrated in figure 10. Figure 7, identifies stagnation regions and the forced vortex. The higher-pressure regions and the vortex alter the aerodynamic geometry of the flow field reducing the effective cross-sectional area, and accelerating the flow through the turn. Therefore the bulk of the flow is guided through this imaginary area induced by the geometry of the duct.

Figure 7 was used to obtain the pressure difference associated with the specific kinetic energy constant. The location on Figure 7 corresponding to the measured pressure was averaged with the pressure near the vortex. The average pressure over that distance is 32 psia.

$$36.3\,\text{psia} = 2.5\text{E}5\,\text{Pa}$$

$$27.7\,\text{psia} = 1.91\text{E}5\,\text{Pa}$$

$$\frac{(36.3 + 27.7)\,\text{psia}}{2} = 32\,\text{psia}$$

The average pressure was subtracted from the measured pressure and divided by two,

$$\frac{(36.3 - 32)\,\text{psia}}{2} = 2.15\,\text{psia}$$

The pressure value can be expressed as,

$$\Delta P = \frac{1}{2}\rho\left(V_2^2 - V_1^2\right) = \frac{1}{2}\rho\left(\Delta V^2\right) = 2.15\,\text{psia}$$

The specific constant is,

$$\frac{\Delta P}{\rho} = \frac{\Delta\left(V^2\right)}{2} = 141{,}590.72\,\frac{\text{ft.}^2}{\text{s}^2} = \beta$$

The corrective differential pressure equation is,

$$\Delta P = \rho\beta$$

Beta represents the specific kinetic energy difference. This correction factor is subtracted from the measured pressure as follows,

$$P_{\text{measured}} - \Delta P = P_{\text{corrected}} = 34.15\,\text{psia}$$

This can be repeated for each test interval over the whole load range. The corrected pressure should be used in the previously described efficiency analysis; the results of the corrected pressure can be seen in figure 16.

Figure 16: IP Turbine efficiency vs. volume flow rate.

The pressure correction model does have limitations, for example if the volume flow rate changes dramatically, the specific kinetic energy difference coefficient must be recalculated. This can be done fairly inexpensively by installing pitot tubes. Any situation where the volume flow rate changes dramatically more than likely indicates that the turbine has under gone a serious mechanical malfunction, which can be verified by the operator's log.

CONCLUSION

Using the pressure correction algorithm is an effective method for accounting for the pressure difference over the load range. However, the installation of more pressure measurement devices to measure the exhaust flow in the appropriate locations will provide a better description of the exhaust pressure. ASME performance test code discusses the proper method for installing measurement devices in the main steam flow. Generally, from an operation and maintenance perspective inline measurement devices are viewed as a liability, but with the proper engineering and precautions the installation of such devices is feasible and practical.

As outlined at the beginning, the primary purpose for this investigation was to determine a pressure correction for the exhaust flow. Upon further investigation the initial efficiency benchmark value was brought under question. The initial benchmark value that was supplied was approximately 91.81%; this value was based on information from a General Electric booklet on turbine efficiency, written by K.C. Cotton. Mr. Cotton was the supervisor of General Electric's Fluid Mechanics Advanced Engineering Program. Mr. Cotton also published a book for the general public titled, "Evaluating and Improving Steam Turbine Performance". This publication contains the same graphs as the GE booklet; however, the book is accompanied with more details. The same graph used to determine the IP turbine efficiency from the GE booklet, is located on page 78 of the book. On

page 79 Mr. Cotton states that the efficiency graph is a conservative approximation, and 0.98 must divide values determined from the graph; doing so yields,

$$\frac{91.81\%}{0.98} = 93.68\%$$

This is approximately the efficiency value being measured without the pressure correction. However, upon consulting with many different field engineers it was determined that an efficiency value of 93.68% is excessive and highly unlikely for a turbine of this vintage. However, this discrepancy is not surprising there are many parameters that can change from the initial test unit at the original equipment manufacture, and equipment installed in the field. This is why an agreement pertaining to guaranteed heat rate between the OEM and the system owner must be met for each individual installation. For this unit the efficiency has never exceeded 92% so the approximation of 91.81% is valid. The pressure correction methodology is a valid engineering model that is based on the flow physics and the turbine design.

Appendix

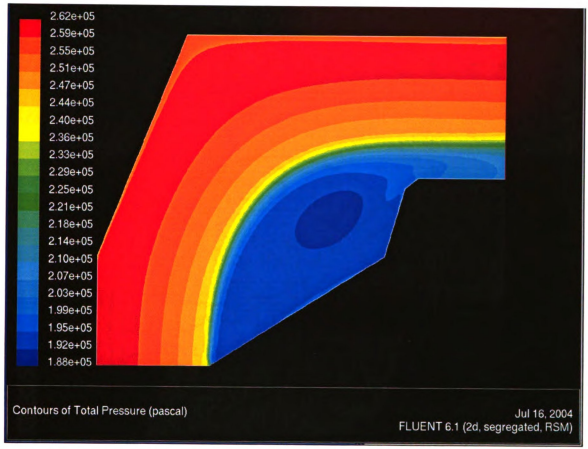

Figure 17: Contours of total pressure.

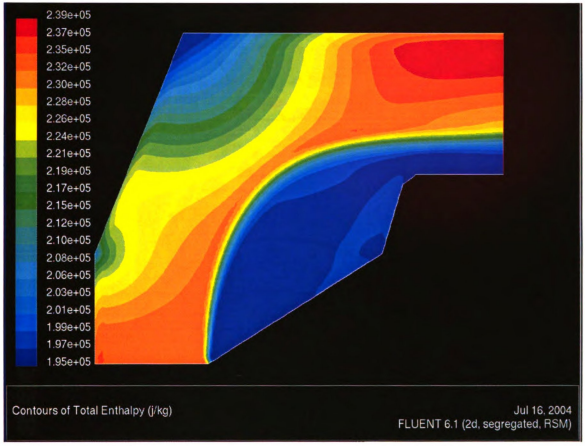

Figure 18: Contours of total enthalpy.

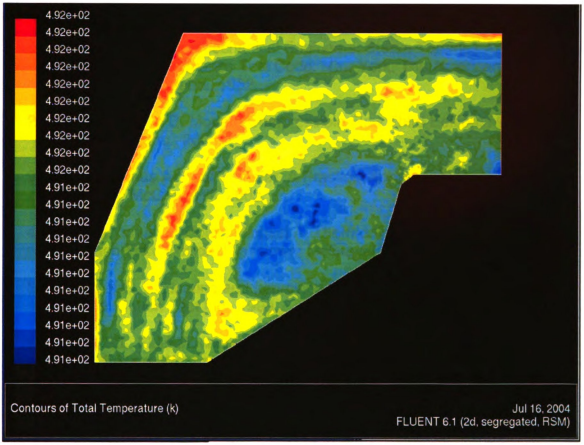

Figure 19: Contours of total temperature.

BIBLIOGRAPHY

1. American Society of Mechanical Engineers. Steam Turbines ANSI/AMSE PTC 6-1976 Performance Test Code. New York: The American Society of Mechanical Engineers, 1982.

2. Anderson, John D. Modern Compressible Flow Third Edition. New York: McGraw-Hill, Inc., 2003.

3. Cengel, Yunus A. Heat Transfer, A Practical Approach Second Edition. New York: McGraw-Hill, 2003.

4. Cengel, Yunus A., Boles, Michael A. Thermodynamics, An Engineering Approach Third Edition. Highstown: McGraw-Hill, Inc., 1998.

5. Cotton, K.C. Evaluating and Improving Steam Turbine Performance. Rexford: Cotton Fact Inc., 1998.

6. Dixion, S.L. Fluid Mechanics and Thermodynamics of Turbomachinery, Fourth Edition. Woburn: Butterworth-Heinemann, 1998.

7. Kearton, William J. Steam Turbine Theory and Practice, Third Edition. London: Sir Issac Pitman & Sons, Ltd., 1931.
8. Munson, Bruce R., Young, Donald F., Okiishi, Theodore H. Fundamentals of Fluid Mechanics Third Edition. New York: John Wiley & Sons, Inc. 1998.

9. Salisbury, J. Kenneth. Steam Turbines and Their Cycles. New York: John Wiley & Sons, Inc., 1950.

10. Stodola, A., Loewenstein, Louis C. Steam and Gas Turbines, Volumes I & II. New York: McGraw-Hill, 1945.

11. Thomas, Jr., George B., Finney, Ross L. Calculus and Analytic Geometry. New York: Addison-Wesley Inc., 1996.